

## Cell death-inducing activities via P-glycoprotein inhibition of the constituents isolated from fruits of *Nandina domestica*

Daisuke Imahori<sup>a</sup>, Takahiro Matsumoto<sup>a,\*</sup>, Youhei Saito<sup>b</sup>, Tomoe Ohta<sup>c</sup>, Tatsusada Yoshida<sup>c</sup>, Yuji Nakayama<sup>b</sup>, Tetsushi Watanabe<sup>a,\*</sup>

<sup>a</sup> Department of Public Health, Kyoto Pharmaceutical University, Misasagi, Yamashina-ku, Kyoto 607-8412, Japan

<sup>b</sup> Department of Biochemistry & Molecular Biology, Kyoto Pharmaceutical University, Misasagi, Yamashina-ku, Kyoto 607-8412, Japan

<sup>c</sup> Faculty of Pharmaceutical Sciences, Nagasaki International University, Nagasaki 859-3298, Japan

### ARTICLE INFO

#### Keywords:

*Nandina domestica*  
Nandinamegastigmane  
ECD prediction  
Adriamycin  
Time-lapse cell imaging  
P-glycoprotein

### ABSTRACT

Two new pyrrole alkaloids methyl-*E*-mangolamide (1) and methyl-*Z*-mangolamide (2), four new megastigmane glycosides nandinamegastigmanes I–IV (3–6), and eight known compounds (7–14) were isolated from the methanol extract of the fruits of *Nandina domestica*. The structures of the new compounds were elucidated based on chemical and spectroscopic evidence. The absolute stereochemistry of nandinamegastigmane I (3) was established upon comparing the experimental and predicted electronic circular dichroism (ECD) data. Among the isolated compounds, 1 and 2 showed cell death-inducing activity on the Adriamycin-treated HeLa cells. In addition, one of the mechanisms for cell death-inducing activity of 1 and 2 was suggested as inhibition of P-glycoprotein.

### 1. Introduction

As a result of long-term and broad research to discover new anticancer drugs from plants, marine organisms, and microorganisms, several types of antimutagenic drugs had been reported to show significant activity. However, these drugs cause damage to normal tissue and have critical side effects. In addition, drug resistance occurs through by DNA repairing [1], mutation of treatment target [2], activation of detoxifying enzymes [3], anti-apoptotic functions of heat shock protein (Hsp) in cancer cells [4], and expression of the drug efflux transporter P-glycoprotein (P-gp) [5]. For example, Adriamycin (ADR) has been used as a potent chemotherapeutic drug for the treatment of several cancers [6]. ADR induces cell death via producing intercalates with base pairs of the DNA's double helix. Although ADR is effective in tumor therapy, the utilities are limited due to side effects such as cardiotoxicity [7]. The compounds which enhance the cytotoxicity of ADR such as inhibitors of P-gp or Hsp, can reduce the dosage of ADR in tumor therapy to avoid the side effects. According to this background, our research group is interested in the naturally occurring compounds that enhance the effect of cancer treatment agents. Previously, we have reported the limonoids and the guaiane type sesquiterpenoids have cell death-inducing activity against the ADR-treated cancer cells [8,9]. During our work, we found

the alkaloids from *Nandina domestica* have cell death-inducing activity on ADR-treated HeLa cells.

*Nandina domestica* Thumb. grows wild in Japan and China and belongs to the family Berberidaceae which comprises 13 genera and 600 species [10]. In Japan, the fruits of this plant, called Nantenjitsu have long been used as a folk medicine for treatment of coughs [11]. In China, they have been used for asthma, whooping cough, pharyngeal tumors, and uterine bleeding [10,12]. The alkaloids [10] and the flavonoids [12] have been isolated and identified from the *N. domestica*. Among them, aporphine-type alkaloids, such as nantenin is the major active component and have been reported to have cytotoxicity. In this study, we isolated six new constituents from *N. domestica* and revealed that two new compounds have cell death-inducing activities under ADR treatment.

### 2. Results and discussion

#### 2.1. Isolation of constituents from fruits of *N. domestica*

The methanol extract of the fruits of *N. domestica* was partitioned in ethyl acetate–H<sub>2</sub>O (1:1, v/v) to furnish an ethyl acetate fraction and aqueous layer. Aqueous layer was further partitioned in *n*-BuOH–H<sub>2</sub>O

\* Corresponding authors.

E-mail addresses: [tmatsumo@mb.kyoto-phu.ac.jp](mailto:tmatsumo@mb.kyoto-phu.ac.jp) (T. Matsumoto), [watanabe@mb.kyoto-phu.ac.jp](mailto:watanabe@mb.kyoto-phu.ac.jp) (T. Watanabe).

<https://doi.org/10.1016/j.fitote.2021.105023>

Received 6 August 2021; Received in revised form 18 August 2021; Accepted 18 August 2021

Available online 21 August 2021

0367-326X/© 2021 Elsevier B.V. All rights reserved.

(1:1, v/v) to furnish an BuOH fraction and H<sub>2</sub>O fraction. The ethyl acetate fraction and BuOH fraction was subjected to normal- and reversed-phase silica gel column chromatography and high-performance liquid chromatography (HPLC) to give six new compounds: methyl-*E*-mangolamide (1, 0.000036%), methyl-*Z*-mangolamide (2, 0.00001%), nandinamegastigmane I (3, 0.00077%), II (4, 0.0008%), III (5, 0.000048%), and IV (6, 0.000071%) together with eight known compounds, (6*S*,9*S*)-roseoside (7, 0.000022%) [13], (6*S*,9*R*)-roseoside (8, 0.000078%) [13], (6*R*,9*R*)-9-hydroxy-4-megastigmen-3-one (9, 0.000016%) [14], (+)-dehydrovomifoliol (10, 0.00001%) [15], loliolide (11, 0.000056%) [16], 4-*O*- $\beta$ -D-glucopyranosylbenzyl-(*E*)-3-(3,4-dihydroxyphenyl)acrylate (12, 0.0009%) [17], 4-*O*- $\beta$ -D-glucopyranosylbenzyl-(*Z*)-3-(3,4-dihydroxyphenyl)acrylate (13, 0.00023%) [17], and 1-*p*-formylphenyl-6-caffeoyl- $\beta$ -D-glucopyranoside (14, 0.00025%) [17].

## 2.2. Structures of new compounds (1–6)

Methyl-*E*-mangolamide (1) and methyl-*Z*-mango amide (2) were isolated as colorless amorphous solid. Their molecular formulas (C<sub>21</sub>H<sub>26</sub>N<sub>2</sub>O<sub>5</sub>) were determined using HRMS and <sup>13</sup>C NMR spectroscopy. A molecular ion peak was observed using EIMS for 1 and 2 (*m/z* 386 [M]<sup>+</sup>). The <sup>1</sup>H and <sup>13</sup>C NMR (CD<sub>3</sub>OD) spectra recorded for 1 and 2 (Table 1) show signals corresponding to a mangolamide [18] group {2-hydroxymethyl-5-formyl pyrrole moiety [1:  $\delta_{\text{H}}$  6.18 (d, *J* = 4.1, H-3), 6.88 (d, *J* = 4.1, H-4), 4.40 (s, H-6), and 9.35 (s, H-7), 2:  $\delta_{\text{H}}$  6.17 (d, *J* = 4.1, H-3), 6.88 (d, *J* = 4.1, H-4), 4.37 (s, H-6), and 9.31 (s, H-7)], 1,4-butanediamine moiety [1:  $\delta_{\text{H}}$  4.26 (t-like, *J* = 7.5, H-1'), 1.69 (t-like, *J* = 7.5, H-2'), 1.50 (t-like, *J* = 7.5, H-3'), and 3.22 (overlapped, H-4'), 2:  $\delta_{\text{H}}$  4.21 (t-like, *J* = 7.6, H-1'), 1.61 (m, H-2'), 1.44 (m, H-3'), and 3.21 (m, H-4')] and ferulamoyl moiety [1:  $\delta_{\text{H}}$  7.02 (d, *J* = 2.1, H-2''), 6.69 (d, *J* = 8.3, H-5''), 6.92 (dd, *J* = 2.1, 8.3, H-6''), 7.32 (d, *J* = 15.2, H-7''), 6.31 (d, *J* = 15.2, H-8''), and 3.79 (s, H-3''-OMe), 2:  $\delta_{\text{H}}$  7.24 (d, *J* = 2.0, H-2''), 6.61 (d, *J* = 8.2, H-5''), 6.82 (dd, *J* = 2.0, 8.2, H-6''), 6.51 (d, *J* = 12.4, H-7''), 5.73 (d, *J* = 12.4, H-7''), and 3.71 (s, H-3''-OMe)]} with a methoxy group {1:  $\delta_{\text{H}}$  3.24 (s, H-6-OMe); 2:  $\delta_{\text{H}}$  3.24 (s, H-6-OMe)}. The positions of each functional groups described above were determined based on the HMBC spectra shown in Fig. 2. Namely, long-range correlations were observed between following pairs; H-1'/C-5, H-4'/C-9'', H-8''/C-9'', H-

**Table 1**

<sup>13</sup>C NMR (150 MHz) and <sup>1</sup>H NMR spectroscopic data (600 MHz) of methyl-*E*-mangolamide (1) and methyl-*Z*-mangolamide (2) recorded in CD<sub>3</sub>OD.

| Position | 1                   |                                       | 2                   |                                       |
|----------|---------------------|---------------------------------------|---------------------|---------------------------------------|
|          | $\delta_{\text{C}}$ | $\delta_{\text{H}}$ ( <i>J</i> in Hz) | $\delta_{\text{C}}$ | $\delta_{\text{H}}$ ( <i>J</i> in Hz) |
| 2        | 142.0               |                                       | 140.9               |                                       |
| 3        | 112.9               | 6.18 (d, 4.1)                         | 112.9               | 6.17 (d, 4.1)                         |
| 4        | 126.0               | 6.88 (d, 4.1)                         | 126.0               | 6.88 (d, 4.1)                         |
| 5        | 133.8               |                                       | 133.8               |                                       |
| 6        | 66.4                | 4.40 (s)                              | 66.4                | 4.37 (s)                              |
| 7        | 181.1               | 9.35 (s)                              | 181.1               | 9.31 (s)                              |
| 1'       | 46.2                | 4.26 (t-like, 7.5)                    | 46.2                | 4.21 (t-like, 7.6)                    |
| 2'       | 29.8                | 1.69 (t-like, 7.5)                    | 29.8                | 1.61 (m)                              |
| 3'       | 27.7                | 1.50 (t-like, 7.5)                    | 27.4                | 1.44 (m)                              |
| 4'       | 40.0                | 3.22 (over lapped solvent signal)     | 39.9                | 3.21 (m)                              |
| 1''      | 128.2               |                                       | 128.5               |                                       |
| 2''      | 111.5               | 7.02 (d, 2.1)                         | 113.8               | 7.24 (d, 2.0)                         |
| 3''      | 149.3               |                                       | 148.5               |                                       |
| 4''      | 149.9               |                                       | 148.5               |                                       |
| 5''      | 116.5               | 6.69 (d, 8.3)                         | 115.8               | 6.61 (d, 8.2)                         |
| 6''      | 123.2               | 6.92 (dd, 2.1, 8.3)                   | 124.8               | 6.82 (dd, 2.0, 8.2)                   |
| 7''      | 141.0               | 7.32 (d, 15.2)                        | 138.1               | 6.51 (d, 12.4)                        |
| 8''      | 118.7               | 6.31 (d, 15.2)                        | 121.7               | 5.73 (d, 12.4)                        |
| 9''      | 169.2               |                                       | 170.4               |                                       |
| 6-OMe    | 58.2                | 3.24 (s)                              | 58.1                | 3.24 (s)                              |
| 3''-OMe  | 56.4                | 3.79 (s)                              | 56.4                | 3.71 (s)                              |

3''-OMe/C-3'', and H-6-OMe/C-6. These correlations suggested the methoxy group is located at C-6 position and ferulamoyl moiety is attached C-4' position by amide bond. The geometry of C-7'' in 1 and 2 were determined by NOESY spectra and coupling constant of H-NMR spectra between H-7'' and H-8'' (1; 15.2 Hz, 2; 12.4 Hz) as *E* for 1 and *Z* for 2 (Fig. 2). Based on this evidence, the chemical structure of methyl-*E*-mangolamide (1) and methyl-*Z*-mangolamide (2) were determined and shown in Fig. 1. In these compounds, the naturally occurred 2-formylpyrrole moiety seems to be synthesized via Maillard reaction that is nonenzymatic reaction of reducing sugars with amines [19].

Nandinamegastigmanes I and II (3 and 4) were isolated as colorless amorphous solid with positive optical rotation 3 ( $[\alpha]_{\text{D}}^{25} + 51.3$  in MeOH) and 4 ( $[\alpha]_{\text{D}}^{25} + 36.7$  in MeOH). The molecular formulas (C<sub>20</sub>H<sub>32</sub>O<sub>8</sub>) were determined using HRMS and <sup>13</sup>C NMR spectroscopy. A molecular ion peak was observed using ESIMS (*m/z* 423 [M + Na]<sup>+</sup>). The <sup>1</sup>H and <sup>13</sup>C NMR (CD<sub>3</sub>OD) spectra recorded for 3 and 4 (Table 2) showed signals similar to roseoside [20] except for the signals due to the atoms around C-9. This analysis and 2D-NMR spectroscopy (Fig. 2) suggested the nandinamegastigmanes I and II (3 and 4) were the megastigmane glucoside having one more carbon atom at side chain than roseoside. The geometry of C-7 in 3 and 4 were determined by NOESY spectra and coupling constant of H-NMR spectra between H-7 and H-8 (1; 15.1 Hz, 2; 9.7 Hz) as *E* for 3 and *Z* for 4 (Fig. 2). Subsequently, acid hydrolysis of 3 and 4 with 20% aqueous H<sub>2</sub>SO<sub>4</sub>-1,4-dioxane yielded D-glucose. D-glucose was identified via HPLC of the chiral tolylthiocarbonyl thiazolidine derivatives of them [21]. The absolute configuration at C-6 was elucidated from experimental and calculated ECD spectra (Fig. 3). The experimental ECD spectrum for 3a obtained via enzymatic hydrolysis from 3 was identical to calculated ECD spectrum of 3b. The chemical structure of 3b have been designed for ECD calculation that assumed to have the same spectra with 3a. The ECD spectrum of 4a obtained from 4 showed similar cotton effect [242.4 nm ( $\Delta\epsilon + 15.5$ )]. This result suggests that the absolute stereo structure at C-6 position of 3 and 4 were *S*. On the basis of all this evidence, the chemical structure of nandinamegastigmanes I and II (3 and 4) were determined and shown in Fig. 1.

Nandinamegastigmane III (5) was isolated as colorless amorphous solid with positive optical rotation ( $[\alpha]_{\text{D}}^{25} + 7.4$  in MeOH). The molecular formulas (C<sub>20</sub>H<sub>32</sub>O<sub>8</sub>) were determined using HRMS and <sup>13</sup>C NMR spectroscopy. The <sup>1</sup>H and <sup>13</sup>C NMR (CD<sub>3</sub>OD) spectra recorded for 5 (Table 2) showed signals similar to nandinamegastigmanes I and II (3 and 4) except for the signals due to the atoms around C-7, 8, 9, 10, and 11. The NMR spectra show signals due to the sidechain corresponding to a methylene group [ $\delta_{\text{H}}$  2.49 (m, H-7a) and 2.65 (overlapping, H-7b)], a olefin group [ $\delta_{\text{C}}$  124.5 (C-8) and 135.4 (C-9)], a methylene bearing

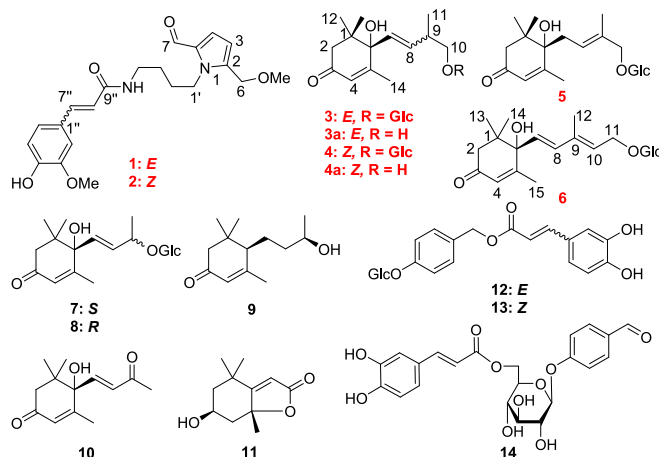


**Fig. 1.** The chemical structures of the constituents (1–14) isolated from fruits of *Nandina domestica*.

**Table 2**<sup>13</sup>C NMR (150 MHz) and <sup>1</sup>H NMR spectroscopic data (600 MHz) of nandinamegastigmanes I–IV (3–6) recorded in CD<sub>3</sub>OD.

| Position | 3          |  | 4          |   | 5          |  | 6          |   |
|----------|------------|--|------------|---|------------|--|------------|---|
|          | $\delta_C$ | $\delta_H$ (J in Hz)                             | $\delta_C$ | $\delta_H$ (J in Hz)                              | $\delta_C$ | $\delta_H$ (J in Hz)                                   | $\delta_C$ | $\delta_H$ (J in Hz)                              |
| 1        | 42.5       |  | 42.5       |   | 42.3       |  | 42.7       |   |
| 2        | 50.8       | $\alpha$ 1.97 (d, 17.2)<br>$\beta$ 2.51 (m)      | 50.1       | $\alpha$ 2.10 (d, 16.5)<br>$\beta$ 2.49 (d, 16.5) | 50.5       | $\alpha$ 2.10 (d, 17.2)<br>$\beta$ 2.64 (over lapping) | 50.7       | $\alpha$ 2.08 (d, 17.2)<br>$\beta$ 2.39 (d, 17.2) |
| 3        | 201.8      |  | 201.5      |   | 201.1      |  | 201.2      |   |
| 4        | 127.2      | 5.79 (s)   | 127.1      | 5.87 (s)  | 127.2      | 5.83 (s)   | 127.1      | 5.80 (s)  |
| 5        | 167.7      |  | 167.7      |   | 170.3      |  | 167.3      |   |
| 6        | 80.4       |  | 80.3       |   | 79.7       |  | 80.4       |   |
| 7        | 131.0      | 5.54 (d, 15.1)                                   | 130.9      | 5.67 (d, 9.7)                                     | 36.5       | a 2.49 (m)<br>b 2.65 (m)                               | 130.0      | 5.71 (d, 15.8)                                    |
| 8        | 135.6      | 5.49 (dd, 7.6, 15.1)                             | 135.5      | 5.68 (m)  | 124.5      | 5.59 (t, 7.6)  | 135.7      | 6.26 (d, 15.8)                                    |
| 9        | 38.2       | 2.47 (m)   | 38.7       | 2.58 (m)  | 135.4      |  | 137.5      |   |
| 10       | 74.9       | a 3.31 (dd, 6.2, 8.9)<br>b 6.67 (t-like, 8.9)    | 75.2       | a 3.77 (dd, 8.9, 6.2)<br>b 3.44 (dd, 6.8, 8.9)    | 75.5       | a 4.01 (d, 8.2)<br>b 4.17 (d, 8.2)                     | 129.4      | 5.61 (d, 7.6)                                     |
| 11       | 17.3       | 0.94 (d, 6.9)                                    | 17.3       | 1.05 (d, 6.2)                                     | 14.4       | 1.65 (s)   | 66.4       | a 4.28 (dd, 7.6, 12.8)<br>b 4.40 (dd, 7.6, 12.8)  |
| 12       | 23.5       | 0.93(s)  | 23.4       | 1.02 (s)  | 24.9       | 0.99 (s)   | 13.0       | 1.73 (s)  |
| 13       | 24.5       | 0.92(s)  | 24.5       | 1.01 (s)  | 24.2       | 1.09 (s)   | 23.5       | 0.95 (s)  |
| 14       | 19.8       | 1.82 (s)   | 19.7       | 1.91 (s)  | 21.2       | 2.00 (s)   | 24.6       | 0.91 (s)  |
| 15       |            |  |            |   |            |  | 19.6       | 1.81 (s)  |
| 1'       | 104.2      | 4.13 (d, 7.6)                                    | 104.4      | 4.23 (d, 8.2)                                     | 102.8      | 4.17 (d, 8.2)  | 103.2      | 4.18 (d, 8.2)                                     |
| 2'       | 75.2       | 3.04 (t, 7.6)                                    | 75.2       | 3.15 (t, 8.2)                                     | 75.1       | 3.15 (t, 8.2)  | 75.1       | 3.08 (t, 8.2)                                     |
| 3'       | 78.0       | 3.13 (m)   | 78.0       | 3.26 (m)  | 77.9       | 3.18 (m)   | 78.1       | 3.19 (m)  |
| 4'       | 71.7       | 3.15 (m)   | 71.7       | 3.24 (m)  | 71.7       | 3.22 (m)   | 71.7       | 3.17 (m)  |
| 5'       | 78.2       | 3.23 (m)   | 78.2       | 3.32 (m)  | 78.1       | 3.31 (m)   | 78.1       | 3.16 (m)  |
| 6'       | 62.8       | a 3.53 (dd, 4.8, 11.6)<br>b 3.74 (dd, 1.2, 11.6) | 62.8       | a 3.63 (dd, 5.5, 12.4)<br>b 3.84 (dd, 1.2, 12.4)  | 62.8       | a 3.63 (dd, 5.5, 11.7)<br>b 3.83 (dd, 1.2, 11.7)       | 62.8       | a 3.56 (dd, 5.6, 12.0)<br>b 3.76 (d-like, 12.0)   |

oxygen function group [ $\delta_H$  4.01 (d,  $J = 8.2$ , H-10a) and 4.17 (d,  $J = 8.2$ , H-10b)], and a methyl group [ $\delta_H$  1.65 (s, H-11)]. Above analysis suggested that the only difference between **3** and **5** was the location of a double bond on the side chain. The position of a double bond described above was determined as C-8/C-9 via HMBC correlations between following pairs; H-10/C-9, H-11/C-8, H-11/C-9, and H-11/C-10 (Fig. 2). Acid hydrolysis of **5** with 20% aqueous H<sub>2</sub>SO<sub>4</sub>-1,4-dioxane yielded D-glucose same as **3** and **4**. Finally, the absolute stereostructure of **5** at C-6 position was deduced as same as **3** and **4**. Based on all this evidence, the chemical structure of nandinamegastigmane III (**5**) was determined and shown in Fig. 1.

Nandinamegastigmane IV (**6**) was isolated as colorless amorphous solid with positive optical rotation ( $[\alpha]_D^{25} + 62.8$  in MeOH). The molecular formulas (C<sub>21</sub>H<sub>32</sub>O<sub>8</sub>) were determined using HRMS and <sup>13</sup>C NMR spectroscopy. Via the <sup>1</sup>H, <sup>13</sup>C, and 2D NMR (CD<sub>3</sub>OD) spectra, the chemical structure of **6** (Table 2) was elucidated as shown Fig. 1. The chemical structure of this compound has been described in previous report however, the chemical structure was deduced only by MS techniques [22]. Therefore, we described several data of this compound such as NMR and MS spectra in this paper. The chemical structure was elucidated by same techniques as other new compounds (1–5).

### 2.3. Evaluation cytotoxicity and cell death analysis

The cytotoxicity of the isolated compounds (1–14) and derivatives (**3a** and **4a**) were evaluated in human cervical cancer (HeLa) cells with or without ADR. The cell viability was examined using crystal violet staining and WST-8 assay. In this assay, tested compounds (1–14, **3a**, and **4a**) did not show cytotoxicity at 60  $\mu$ M for 24 h (Fig. 4A). However, combination treatment of **1** and **2** (60  $\mu$ M) with ADR (1  $\mu$ g/mL) showed stronger cytotoxicity than that of the only ADR (1  $\mu$ g/mL) treatment on the crystal violet staining and WST-8 assay (Fig. 4B, C). On the WST-8 assay, IC<sub>50</sub> value of ADR (IC<sub>50</sub> of ADR: 1.69  $\pm$  0.11  $\mu$ M) was significantly decreased by treatment of **1** (IC<sub>50</sub> of ADR: 0.72  $\pm$  0.04  $\mu$ M) or **2** (IC<sub>50</sub> of ADR: 0.65  $\pm$  0.08  $\mu$ M) ( $p < 0.001$ ) (Fig. 4D, E). These results suggested that the compounds **1** and **2** may be able to decrease the amount of ADR for cancer treatment.

Only using cell viability assay, it is difficult to evaluate whether the

cytotoxicity was caused by cell death or cell cycle arrest. Therefore, we performed time-lapse cell imaging analysis using living HeLa cells as previously reported [8,9,23]. In the control and the tested compounds (1–14, **3a**, and **4a**) treated cells, almost all cells progressed to the mitotic phase within 24 h, whereas the ADR-treated cells did not enter mitosis (Fig. 5A, B). However, around 70% of cells were not died by ADR treatment at a concentration of 1  $\mu$ g/mL. Interestingly, the compounds **1** and **2** significantly increased the number of dead cells under ADR treatment ( $p < 0.001$ ) (Fig. 5A, B). Compounds **1** and **2** showed almost the same activities; therefore, the geometry of C-7'' did not affect the cell death-inducing activity of ADR. According to the above results, **1** and **2** were selected as potential agents among tested compounds as cell death-inducing activity of ADR. Among the megastigmane group (**3**, **3a**, **4**, and **4a**), the sugar moieties were found to decrease the cell death-inducing activity on ADR treated cells.

### 2.4. Evaluation of the drug efflux activity by P-glycoprotein (P-gp) on compound **1** and **2** treated HeLa cells

P-gp is a member of the human ATP-binding cassette (ABC) family and causes drug resistance in cancer cells [24,25]. These ABC transporters have been suggested to transport anticancer drugs, including Anthracyclines [26], Vinca alkaloids [27], and some molecular targeted drugs [28] such as imatinib, erlotinib, and sunitinib. Epidemiological studies have shown that MDR 1 gene is overexpressed in many tumors [29]. Therefore, the overexpression of the ABC transporter has been linked to clinical multidrug resistance in solid tumors and blood cancers, which remains a significant obstacle to successful cancer chemotherapy [30]. The HeLa cells expressing P-gp and it relates to drug resistance [31]. We further examined the inhibitory effects of **1** and **2** against P-gp in HeLa cells by Operetta high-content imaging system. We used Rhodamine 123 (Rh 123) as an artificial substrate of P-gp [32] and the amounts of Rh 123 in living cells were evaluated by fluorescence intensity. For positive control, verapamil was used as P-gp inhibitor [33]. In the control group, after co-culture with Rh 123, relative fluorescence intensity was decreased to 58.9% (3 h) and 24.1% (6 h). On the other hand, verapamil, **1**, and **2** suppressed the decrement of relative fluorescence intensity as 99.0% (verapamil), 67.3% (**1**), and 57.9% (**2**) of

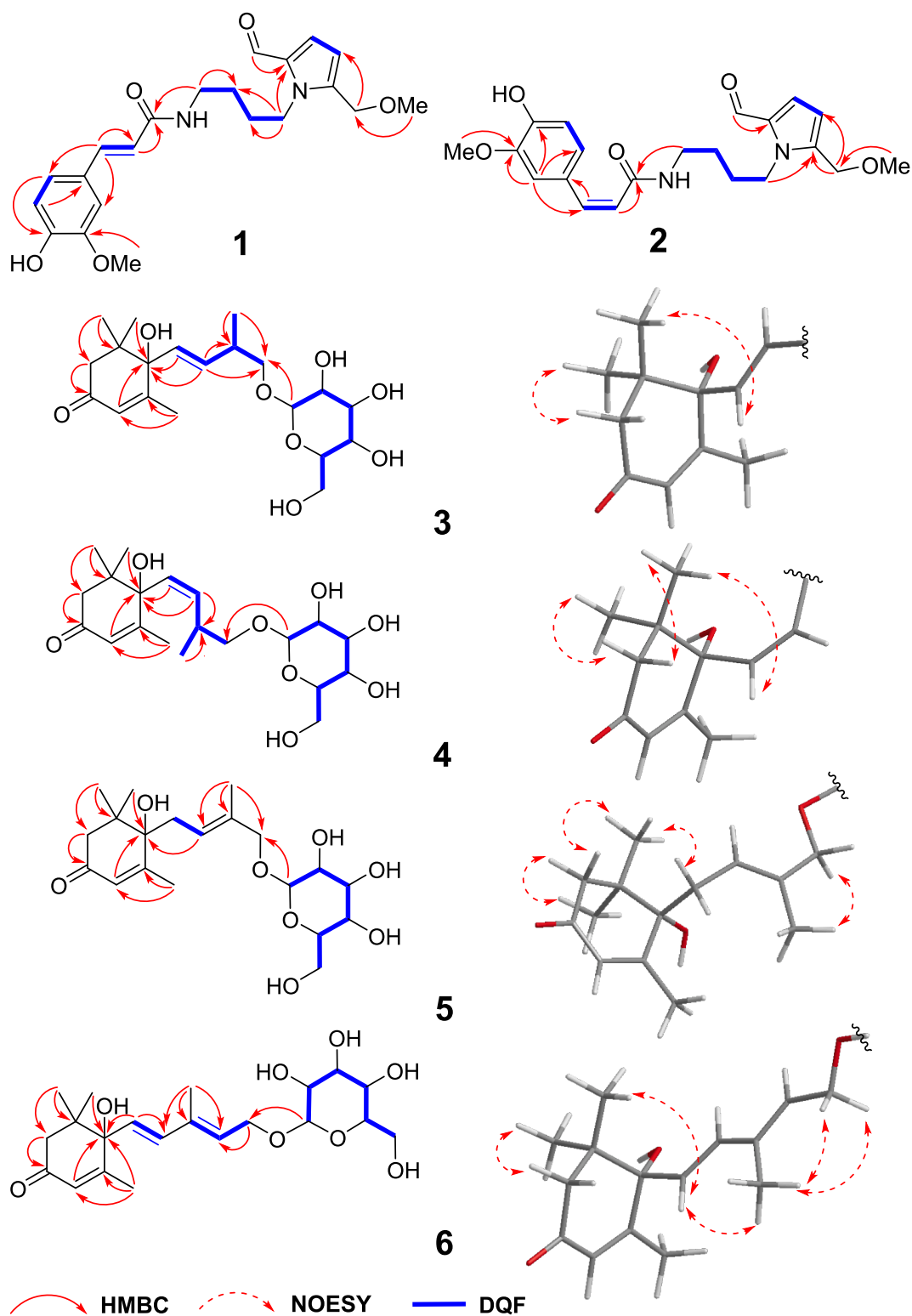


Fig. 2. The important 2D NMR and NOESY correlations for new compounds (1–6).

the intensities were still observed after 6 h, resulting that the Rh 123 efflux inhibition rate was 98.7% (verapamil), 56.9% (1), and 44.6% (2) (Fig. 6). In these experiments, test compounds did not affect the cell proliferation at 30  $\mu\text{M}$  and 60  $\mu\text{M}$ . These results suggests that the inhibition of P-gp activity may be one of the mechanisms of cell death-inducing activity of 1 and 2 on ADR-treated cells.

### 3. Experimental section

#### 3.1. General experimental procedures

Specific rotations were obtained on a JASCO P-2200 digital polarimeter ( $l = 5$  cm) (JASCO, Tokyo, Japan). FTIR spectra were recorded on a JASCO FT/IR-4600 Fourier transform infrared spectrometer (JASCO). ECD spectroscopy was recorded on a JASCO J-1500 spectrometer

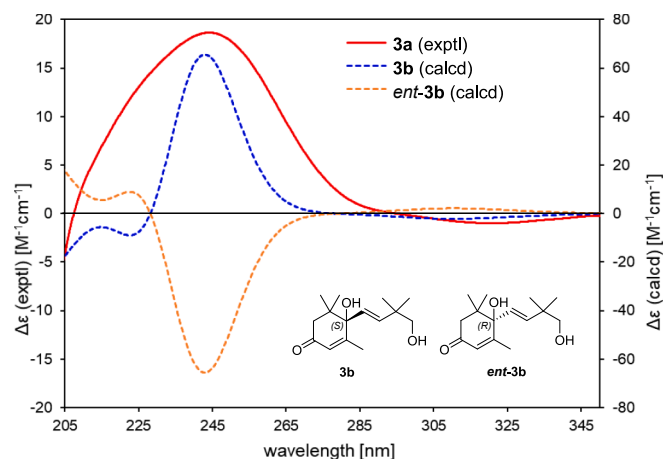


**Fig. 3.** A comparison of the experimental (3a) and calculated (3b and ent-3b) ECD spectra.

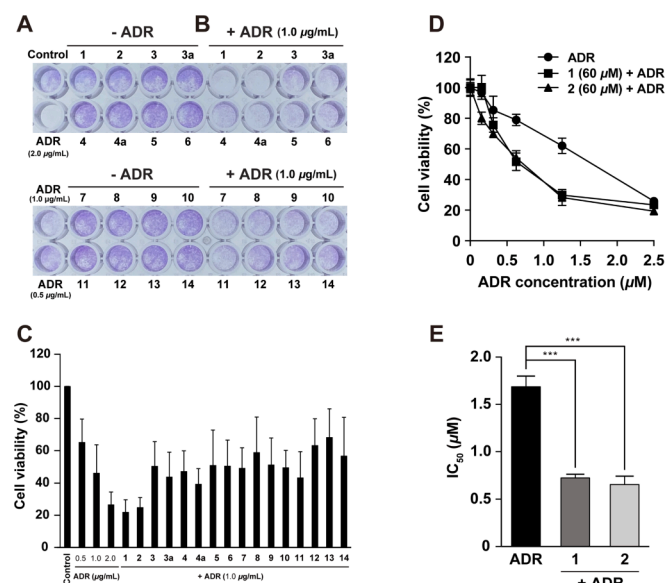


**Fig. 4.** The cytotoxic effects of the isolated compounds (1–14) and derivatives (3a and 4a): (A–E) (A) HeLa cells were treated with 60  $\mu\text{M}$  of the indicated compounds or 0.5, 1, 2  $\mu\text{g}/\text{mL}$  of ADR for 24 h and subjected to crystal violet staining. ADR was used as a positive control. (B) Crystal violet staining of HeLa cells treated with 60  $\mu\text{M}$  of the indicated compounds in combination with ADR for 24 h. (C) The percentage cell viability measured by crystal violet staining was reported as the mean  $\pm$  SD of three independent experiments. (D, E) HeLa cells were seeded into 96-well plates (3000 cells/well) and cultured at 37  $^{\circ}\text{C}$ . After 24 h, ADR was added to the culture medium at varying concentrations of 0–2.5  $\mu\text{M}$  with or without 60  $\mu\text{M}$  of compounds 1 and 2, and cells were cultured at 37  $^{\circ}\text{C}$  for 24 h. (D) Surviving cells were detected by WST-8 assay. Data are expressed as means  $\pm$  S.D. in triplicate experiments. Data are representative of at least three independent experiments. (E)  $\text{IC}_{50}$  values are expressed as mean  $\pm$  S.D. Statistical significance was analyzed using the Tukey–Kramer test. (\*\*\*)  $P < 0.001$  compared with DMSO-treated cells. (For interpretation of the references to colour in this figure legend, the reader is referred to the web version of this article.)

(JASCO). ESIMS and high-resolution ESIMS was recorded on a Shimadzu LCMS-IT-TOF (Shimadzu, Kyoto, Japan). EIMS and HREIMS were recorded on JEOL JMS-GCMATE mass spectrometer (JEOL, Tokyo, Japan).  $^1\text{H}$  NMR spectroscopy was recorded on JEOL ECS400 (400 MHz) and JNM-ECA 600 (600 MHz) spectrometers (JEOL).  $^{13}\text{C}$  NMR spectroscopy was recorded on a JNM-ECA 600 (150 MHz) spectrometer (JEOL). 2D-NMR experiments were carried out on a JEOL JNM-ECA 600

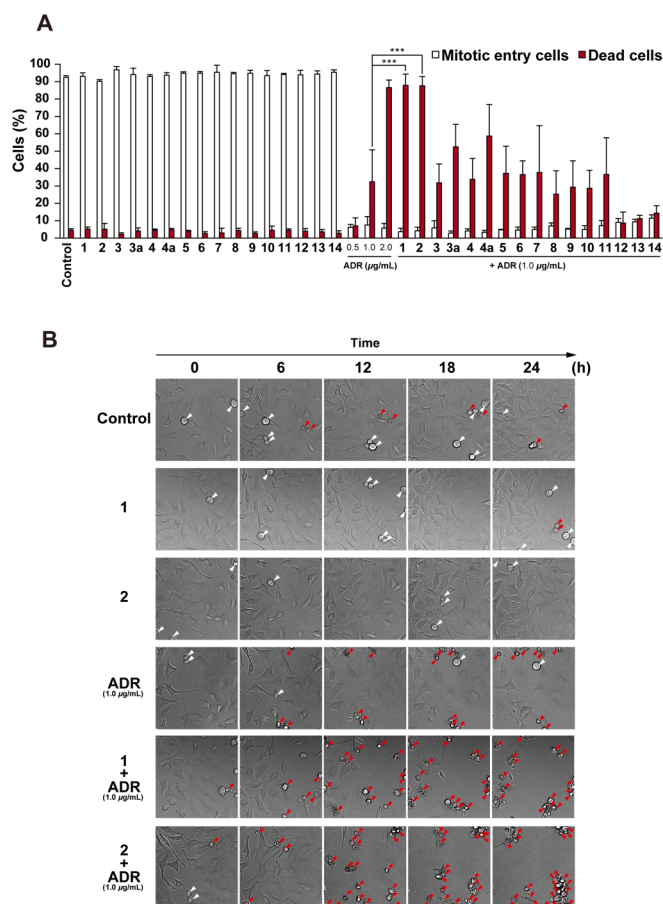


**Fig. 5.** The time lapse imaging analysis of the isolated compounds (1–14) and derivatives (3a and 4a): (A, B) HeLa cells treated with 60  $\mu\text{M}$  of the indicated compounds or 0.5, 1.0, 2.0  $\mu\text{g}/\text{mL}$  of ADR for 24 h. During these treatments, the changes in the cell morphology were determined using time-lapse recording. (A) The percentages of mitotic entry cells (white columns) or dead cells (red columns) are reported as the mean  $\pm$  S.D. of three independent experiments. Statistical significance was analyzed using the Tukey–Kramer test. (\*\*\*)  $P < 0.001$  compared with 1  $\mu\text{g}/\text{mL}$  of ADR-treated cells. (B) Representative images are shown. White arrowheads indicate the mitotic cells and red arrowheads indicate dead cells. (For interpretation of the references to colour in this figure legend, the reader is referred to the web version of this article.)

(600 MHz) spectrometer (JEOL).

Normal-phase silica gel column chromatography was carried out using Silica gel 60 (63–210 mesh) (Kanto Chemical, Tokyo, Japan) and reversed-phase silica gel column chromatography was carried out on C18-OPN (140  $\mu\text{m}$ ) (Nacalai Tesque, Kyoto, Japan). Thin-layer chromatography (TLC) was performed using TLC plates pre-coated with 60F254 silica gel (0.25 mm; ordinary phase) (Merck, Darmstadt, Germany) and RP-18 F254S silica gel (0.25 mm; reversed-phase) (Merck). Reversed-phase high-performance TLC was carried out using TLC plates pre-coated with RP-18 WF254S silica gel (0.25 mm) (Merck). HPLC was performed using a Shimadzu SPD-M10Avp UV–vis detector (Shimadzu). COSMOSIL 5C18-MS-II (250  $\times$  4.6 mm i.d. and 250  $\times$  20 mm i.d.) (Nacalai Tesque) and YMC-Triart PFP (250  $\times$  4.6 mm i.d. and 250  $\times$  20 mm i.d.) (YMC, Kyoto, Japan) columns were used for analytical and preparative purposes.

### 3.2. Plant material

The fruits of *N. domestica* distributed in the Nara prefecture of Japan were purchased from Tochimoto tenkaido (Osaka prefecture, Japan) in November 2019.

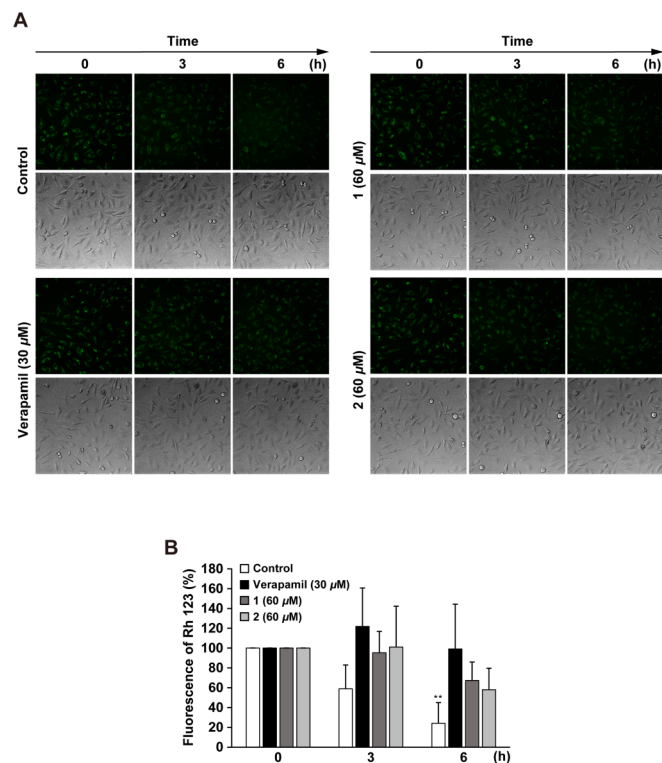


**Fig. 6.** Effects of isolated compound **1** and **2** on the efflux inhibition of Rh 123: (A) HeLa cells were incubated with Rh 123 (1 μM) for 2 h. After removal of Rh123, cells were treated with verapamil (30 μM), compounds **1** and **2** (60 μM) or DMSO for 6 h, and fluorescence was detected by Operetta cell imaging system. Data are representative of at three independent experiments. (B) The percentages of Rh 123 fluorescence are shown as means ± S.D. of three independent experiments. The intensity of fluorescence was quantified at the same field at 0–6 h as described in the “Experimental section”. Each graph was normalized with the 0-h time point as 100%. Statistical significance was analyzed using Dunnett’s test (\*\**P* < 0.01 compared with DMSO-treated cells).

### 3.3. Extraction and isolation

The dried fruits of *N. domestica* (5 kg) were extracted three times with methanol under reflux for 3 h. Evaporation of the solvent provided a methanol extract (1160 g, 23.2%). The methanol extract was partitioned into ethyl acetate–water (1:1, v/v) to furnish an ethyl acetate fraction (40.6 g, 0.81%) and water-soluble fraction. The water-soluble fraction was further partitioned into *n*-BuOH–water (1:1, v/v) to furnish a BuOH fraction (111.7 g, 2.2%) and H<sub>2</sub>O fraction. The ethyl acetate-soluble fraction was subjected to normal-phase silica gel column chromatography [1200 g, *n*-hexane–CHCl<sub>3</sub> (1:1 → 1:5, v/v) → CHCl<sub>3</sub>–MeOH (1:0 → 50:1 → 20:1 → 10:1 → 1:1, v/v)] to give eight fractions (EA1–EA8). Fraction EA4 (1.4 g) was separated using reversed-phase silica gel column chromatography to give seven fractions. Fraction EA4–3 (72.5 mg) was purified using HPLC {H<sub>2</sub>O–CH<sub>3</sub>CN (80:20, v/v)} to give **10** (5.2 mg) and **11** (2.8 mg). Fraction EA4–4 (36.6 mg) was purified using HPLC {H<sub>2</sub>O–CH<sub>3</sub>CN (80:20, v/v)} to give **9** (0.8 mg). Fraction EA5 (3.0 g) was separated using reversed-phase silica gel column chromatography to give nine fractions. Fraction EA5–4 (163.6 mg) was purified using HPLC {H<sub>2</sub>O–CH<sub>3</sub>CN–CH<sub>3</sub>COOH (65:35:0.3, v/v/v)} to give **1** (1.8 mg) and **2** (0.5 mg). The part of BuOH fraction (60.0 g) was subjected to normal-phase silica gel column chromatography [1200 g, *n*-hexane–CHCl<sub>3</sub> (1:1 → 1:4, v/v) → CHCl<sub>3</sub>–MeOH (1:0 → 50:1 → 40:1 → 30:1 → 20:1 → 10:1 → 1:1, v/v)] to give eight fractions (B1–B8). Fraction B6 (5.8 g) was separated using reversed-phase silica gel column chromatography to give ten fractions. Fraction B6–3 (383.3 mg) was purified using HPLC {H<sub>2</sub>O–CH<sub>3</sub>CN (90:10, v/v)} to give **7** (0.6 mg) and **8** (2.1 mg). Fraction

B6–4 (474.2 mg) was purified using HPLC {H<sub>2</sub>O–CH<sub>3</sub>CN (85:15, v/v)} to give **3** (20.8 mg), **4** (21.6 mg), **5** (1.3 mg), and **6** (1.9 mg). Fraction B7 (17.3 g) was separated using reversed-phase silica gel column chromatography to give nine fractions. Fraction B7–4 (223.4 mg) was purified using HPLC {H<sub>2</sub>O–CH<sub>3</sub>CN (80:20, v/v)} to give **12** (24.1 mg), **13** (6.2 mg), and **14** (6.6 mg).

### 3.4. Methyl-*E*-mangolamide (**1**)

Amorphous powder; <sup>1</sup>H NMR (CD<sub>3</sub>OD, 600 MHz) and <sup>13</sup>C NMR (CD<sub>3</sub>OD, 150 MHz), see Table 1; EIMS *m/z* 386 [M]<sup>+</sup>; HREIMS *m/z* 386.1845 [M + Na]<sup>+</sup> (calcd for C<sub>21</sub>H<sub>26</sub>N<sub>2</sub>O<sub>5</sub>, 386.1842).

### 3.5. Methyl-*Z*-mangolamide (**2**)

Amorphous powder; <sup>1</sup>H NMR (CD<sub>3</sub>OD, 600 MHz) and <sup>13</sup>C NMR (CD<sub>3</sub>OD, 150 MHz), see Table 1; EIMS *m/z* 386 [M]<sup>+</sup>; HREIMS *m/z* 386.1841 [M + Na]<sup>+</sup> (calcd for C<sub>21</sub>H<sub>26</sub>N<sub>2</sub>O<sub>5</sub>, 386.1842).

### 3.6. Nandinamegastigmane I (**3**)

Amorphous powder; [α]<sub>D</sub><sup>25</sup> + 51.3 (c 0.1, MeOH); <sup>1</sup>H NMR (CD<sub>3</sub>OD, 600 MHz) and <sup>13</sup>C NMR (CD<sub>3</sub>OD, 150 MHz), see Table 2; ESIMS *m/z* 423 [M + Na]<sup>+</sup>; HRESIMS *m/z* 423.1994 (calcd for C<sub>20</sub>H<sub>32</sub>O<sub>8</sub>Na [M + Na]<sup>+</sup>, 423.1989).

### 3.7. Nandinamegastigmane II (**4**)

Amorphous powder; [α]<sub>D</sub><sup>25</sup> + 36.7 (c 0.1, MeOH); <sup>1</sup>H NMR (CD<sub>3</sub>OD, 600 MHz) and <sup>13</sup>C NMR (CD<sub>3</sub>OD, 150 MHz), see Table 2; ESIMS *m/z* 423 [M + Na]<sup>+</sup>; HRESIMS *m/z* 423.1991 (calcd for C<sub>20</sub>H<sub>32</sub>O<sub>8</sub>Na [M + Na]<sup>+</sup>, 423.1989).

### 3.8. Nandinamegastigmane III (**5**)

Amorphous powder; [α]<sub>D</sub><sup>25</sup> + 7.4 (c 0.3, MeOH); <sup>1</sup>H NMR (CD<sub>3</sub>OD, 600 MHz) and <sup>13</sup>C NMR (CD<sub>3</sub>OD, 150 MHz), see Table 2; ECD: Δε (nm) -2.80 (199.4), +0.52 (214.0), -0.18 (234.7), +0.49 (268.1) (MeOH); ESIMS *m/z* 423 [M + Na]<sup>+</sup>; HRESIMS *m/z* 423.1984 (calcd for C<sub>20</sub>H<sub>32</sub>O<sub>8</sub>Na [M + Na]<sup>+</sup>, 423.1989).

### 3.9. Nandinamegastigmane IV (**6**)

Amorphous powder; [α]<sub>D</sub><sup>25</sup> + 62.8 (c 0.3, MeOH); <sup>1</sup>H NMR (CD<sub>3</sub>OD, 600 MHz) and <sup>13</sup>C NMR (CD<sub>3</sub>OD, 150 MHz), see Table 2; ECD: Δε (nm) -2.2 (221.7), +2.4 (250.3) (MeOH); ESIMS *m/z* 435 [M + Na]<sup>+</sup>; HRESIMS *m/z* 435.1984 (calcd for C<sub>21</sub>H<sub>32</sub>O<sub>8</sub>Na [M + Na]<sup>+</sup>, 435.1989).

### 3.10. Acid hydrolysis of nandinamegastigmanes I–IV (**3–6**)

The solution of **3–6** (each 0.5 mg) in 20% aqueous H<sub>2</sub>SO<sub>4</sub>–1,4-dioxane were heated 90 °C and stirred for 2 h with a reflux condenser. After the acid hydrolysis of **3–6**, solutions were neutralized and extracted with EtOAc and H<sub>2</sub>O. After drying in vacuo, H<sub>2</sub>O soluble fraction was dissolved in pyridine (0.1 mL) containing L-cysteine methyl ester hydrochloride (0.5 mg) and heated at 60 °C for 1 h. A solution of *o*-tolylisothiocyanate (0.5 mg) in pyridine (0.1 mL) was added, and the mixture was heated at 60 °C for 1 h. The mixture was analyzed by reversed-phase HPLC [column: COSMOSIL 5C18-AR-II, 250 × 4.6 mm i. d. (5 μm); mobile phase: 20% CH<sub>3</sub>CN in 50 mM H<sub>3</sub>PO<sub>4</sub>; detection: UV (254 nm); flow rate: 1.0 mL/min; column temperature: 25 °C] to identify the derivatives of constituent *D*-glucose by comparison of their retention times with those of authentic samples (RT: *D*-glucose, 37.5 min; *L*-glucose, 29.9 min).

### 3.11. Enzymatic hydrolysis of nandinamegastigmanes I and II (3 and 4)

The solution of **3** or **4** (each 5 mg) in 20 mM acetate buffer (3.0 mL, pH = 5.0) were added  $\beta$ -glucosidase (2 mg, from Sweet almond) and the mixtures were stirred for 24 h at 37 °C. The supernatant solutions were concentrated under vacuum to give the residues, which were subjected to HPLC {COSMOSIL 5C18-MS-II, H<sub>2</sub>O-CH<sub>3</sub>CN (70:30, v/v)} to give **3a** (1.3 mg) or **4a** (0.8 mg).

### 3.12. Aglycone of 3 (3a)

Amorphous powder;  $[\alpha]_D^{25} + 64.7$  (c 0.26, MeOH); <sup>1</sup>H NMR (CDCl<sub>3</sub>, 600 MHz),  $\delta$  2.22 (d,  $J = 17.2$ , H-2), 2.43 (d,  $J = 17.2$ , H-2), 5.91 (s, H-4), 5.62 (d,  $J = 15.8$ , H-7), 5.66 (dd,  $J = 15.8, 6.8$ , H-8), 2.45 (m, H-9), 3.47 (m, H-10), 3.54 (m, H-10), 1.04 (d,  $J = 6.9$ , H-11), 1.08 (s, H-12), 1.01 (s, H-13), 1.90 (s, H-14); <sup>13</sup>C NMR (CDCl<sub>3</sub>, 150 MHz);  $\delta$  41.1 (C-1), 49.8 (C-2), 198.1 (C-3), 126.9 (C-4), 162.9 (C-5), 79.3 (C-6), 130.4 (C-7), 134.3 (C-8), 39.4 (C-9), 67.3 (C-10), 16.5 (C-11), 22.9 (C-12), 24.1 (C-13), 19.0 (C-14); EIMS  $m/z$  238 [M]<sup>+</sup>; HREIMS  $m/z$  238.1568 (calcd for C<sub>14</sub>H<sub>22</sub>O<sub>3</sub> [M]<sup>+</sup>, 238.1569).

### 3.13. Aglycone of 4 (4a)

Amorphous powder;  $[\alpha]_D^{25} + 63.7$  (c 0.5, MeOH); <sup>1</sup>H NMR (CDCl<sub>3</sub>, 600 MHz),  $\delta$  2.22 (d,  $J = 17.2$ , H-2), 2.43 (d,  $J = 17.2$ , H-2), 5.91 (s, H-4), 5.64 (d,  $J = 6.0$ , H-7), 5.64 (m, H-8), 3.48 (m, H-9), 3.47 (m, H-10), 3.55 (m, H-10), 1.02 (d,  $J = 6.9$ , H-11), 1.08 (s, H-12), 1.02 (s, H-13), 1.90 (s, H-14); <sup>13</sup>C NMR (CDCl<sub>3</sub>, 150 MHz);  $\delta$  41.1 (C-1), 49.7 (C-2), 198.1 (C-3), 126.9 (C-4), missing (C-5), 79.3 (C-6), 130.5 (C-7), 134.3 (C-8), 39.6 (C-9), 67.3 (C-10), 16.6 (C-11), 22.9 (C-12), 24.1 (C-13), 18.9 (C-14); ESIMS  $m/z$  239 [M]<sup>+</sup>; HRESIMS  $m/z$  239.1617 (calcd for C<sub>14</sub>H<sub>23</sub>O<sub>3</sub> [M + H]<sup>+</sup>, 239.1642).

### 3.14. Calculation of the theoretical ECD spectra of 3b

The initial geometries of conformers for enantiomer, **3b** (6S) and *ent*-**3b** (6R), were generated and then geometrically optimized in vacuum by using the Merck molecular force field (MMFF) as implemented in Spartan '10 program [34]. The initial low-energy conformers for each enantiomer with Boltzmann distributions over 1% were further optimized and verified stability at the CAM-B3LYP/6-31G(d) level of long-range corrected density functional theory (DFT). The 20 low-energy conformers for each enantiomer with Boltzmann distributions over 1% were subjected to the ECD calculations using time-dependent density functional theory (TD-DFT) at the CAM-B3LYP/def2-TZVP level. Geometry optimizations and ECD calculations were both carried out with an integral equation formalism polarizable continuum model (IEFPCM) in MeOH using Gaussian 16 program [35]. The calculated ECD curves were generated using SpecDis v1.71 [36].

### 3.15. Cells

Human cervical carcinoma (HeLa) cells were maintained in Dulbecco's modified Eagle's medium (DMEM) with low glucose (Wako Pure Chemical Industries, Osaka, Japan) supplemented with 5% fetal bovine serum (Sigma-Aldrich, St Louis, MO, USA) under a 5% CO<sub>2</sub> atmosphere at 37 °C.

### 3.16. Crystal violet staining

Crystal violet staining was performed described previously [8]. Briefly, cells were fixed and stained with 100  $\mu$ L of 50% methanol containing 0.5% (v/v) crystal violet solution (V5265; Sigma-Aldrich) for 5 min. After fixation and staining, the mixture was removed and washed with tap water. The plates were dried at room temperature. Cell viability was measured following crystal violet staining. Fixed and stained cells

were solubilized in 100  $\mu$ L methanol and absorbance was detected at 595 nm using a microplate reader (Sunrise Thermo RC-R; Tecan Austria GmbH, Grodig, Austria).

### 3.17. WST-8 assay

Cell viability was determined using a cell counting kit 8 (CCK-8; Dojindo, Kumamoto, Japan) method as described previously [8]. Briefly, cells were seeded in 96-well cell culture plates. After approximately 24 h, the cells were treated with ADR (Wako Pure Chemical Industries) with or without isolated compounds (60  $\mu$ M) for 24 h. The absorbance was measured at 450 and 650 nm using a microplate reader. Values for the concentration that inhibited growth by 50% (IC<sub>50</sub>) were calculated using GraphPad Prism 8.43 (GraphPad Software, San Diego, CA, USA).

### 3.18. Time-lapse imaging

Time-lapse imaging was performed on an Operetta high-content imaging system (PerkinElmer, Waltham, MA, USA) as described previously [8,9,21]. Briefly, the cells were cultured in a flat-bottomed 96-well plate (Coster 3596; Corning, NY, USA) to reach 70–80% confluence. The cells were then treated with compound **1–14** and ADR just prior to the time-lapse cell imaging. The images were captured at 10 min intervals for 24 h under a 5% CO<sub>2</sub> atmosphere at 37 °C.

### 3.19. Evaluation of the activity of P-glycoprotein on HeLa cells

In this assay, we observed the green fluorescence of Rh 123 (Wako Pure Chemical Industries) to evaluate the efflux activity of P-gp. The exponentially growing HeLa cells were seeded into 24-well plates (Coster 3526; Corning) at a density of  $8 \times 10^4$  cells/mL in a final volume of 500  $\mu$ L medium for 12 h. After incubation, the culture medium was replaced to medium containing Rh 123 (1  $\mu$ M), and the cells were cultured in the dark for 2 h under a 5% CO<sub>2</sub> atmosphere at 37 °C. Then, the cells were washed with fresh ice-cold medium three times to remove non-absorbed Rh 123 and incubated with or without 60  $\mu$ M of individual isolated compounds (**1** and **2**) and verapamil (V4629; Sigma-Aldrich) as a positive control just prior to the time-lapse cell imaging. The images were captured at 30 min intervals for 6 h under a 5% CO<sub>2</sub> atmosphere at 37 °C. Fluorescence images were obtained with an Operetta high-content imaging system (PerkinElmer). The excitation and emission wavelengths were 460–490 nm and 500–550 nm, respectively. The images were observed and examined using 20  $\times$  objective. Lamp power and exposure time were set and kept constant throughout each experiment to avoid overexposure of the fluorescence signal. Figures were prepared with Photoshop 2021 (Adobe, San Jose, CA, USA) and Illustrator 2021 (Adobe). Integrated fluorescence intensity was determined by ImageJ software (NIH, USA) from the images of three independent experiments.

### 3.20. Statistical analysis

Statistical analyses were performed using GraphPad Prism 8.43 software. The statistical analysis was conducted using one-way analysis of variance (ANOVA) followed by a Tukey-Kramer or Dunnett's test to analyze the differences between the treatment groups. The differences were considered significant when \*\*\* $P < 0.001$  or \*\* $P < 0.01$ .

### Contribution

conceptualization: T. Matsumoto; Data curation: D. Imahori, T. Matsumoto, Y. Saito, T. Ohta; Formal analysis, Visualization, Investigation, Validation, and Writing - original draft: D. Imahori, T. Matsumoto; Funding acquisition: T. Matsumoto; Methodology: T. Matsumoto, Y. Saito; Project administration: Y. Nakayama, T. Watanabe; Resources and

Software: T. Matsumoto, T. Yoshida, Y. Nakayama; Supervision and Writing - review & editing: All authors.

## Declaration of Competing Interest

The authors declare no competing financial interest.

## Acknowledgements

This work was supported by JSPS KAKENHI Grant Numbers 20H03397 (for T.M.) and 20J14567 (for D.I.).

## Appendix A. Supplementary data

Experimental details including the 1D and 2D NMR spectra of new compounds and DFT-optimized structures of the conformers of compound **3b** are available in the supporting information. Supplementary data to this article can be found online at <https://doi.org/10.1016/j.fitote.2021.105023>.

## References

- M. Miyaki, T. Ono, S. Hori, H. Umezawa, Binding of bleomycin to DNA in bleomycin-sensitive and-resistant rat ascites hepatoma cells, *Cancer Res.* 35 (8) (1975) 2015–2019.
- W.G. Harker, D.L. Slade, R.L. Parr, P.W. Feldhoff, D.M. Sullivan, M.H. Holguin, Alterations in the topoisomerase IIa gene, messenger RNA, and subcellular protein distribution as well as reduced expression of the DNA topoisomerase  $\eta$  enzyme in a mitoxantrone-resistant HL-60 human leukemia cell line, *Cancer Res.* 55 (8) (1995) 1707–1716.
- Y. Kondo, E.S. Woo, A.E. Michalska, K.H. Choo, J.S. Lazo, Metallothionein null cells have increased sensitivity to anticancer drugs, *Cancer Res.* 55 (10) (1995) 2021–2023.
- T. Yamane, Y. Saito, H. Teshima, M. Hagino, A. Kakihana, S. Sato, M. Shimada, Y. Kato, T. Kuga, N. Yamagishi, Y. Nakayama, Hsp105 $\alpha$  suppresses Adriamycin-induced cell death via nuclear localization signal-dependent nuclear accumulation, *J. Cell. Biochem.* 120 (10) (2019) 17951–17962, <https://doi.org/10.1002/jcb.29062>.
- G. Szakács, J.K. Paterson, J.A. Ludwig, C. Booth-Genthe, M.M. Gottesman, Targeting multidrug resistance in cancer, *Nat. Rev. Drug Discov.* 5 (3) (2006) 219–234, <https://doi.org/10.1038/nrd1984>.
- R.M. Damiani, D.J. Moura, C.M. Viau, R.A. Caceres, J.A.P. Henriques, J. Saffi, Pathways of cardiac toxicity: comparison between chemotherapeutic drugs doxorubicin and mitoxantrone, *Arch. Toxicol.* 90 (9) (2016) 2063–2076, <https://doi.org/10.1007/s00204-016-1759-y>.
- K.G. Cheung, L.K. Cole, B. Xiang, K. Chen, X. Ma, Y. Myal, G.M. Hatch, Q. Tong, V. W. Dolinsky, Sirtuin-3 (SIRT3) protein attenuates doxorubicin-induced oxidative stress and improves mitochondrial respiration in H9c2 cardiomyocytes, *J. Biol. Chem.* 290 (17) (2015) 10981–10993, <https://doi.org/10.1074/jbc.M114.607960>.
- T. Kitagawa, T. Matsumoto, D. Imahori, M. Kobayashi, M. Okayama, T. Ohta, T. Yoshida, T. Watanabe, Limonoids isolated from the *Fortunella crassifolia* and the *Citrus junos* with their cell death-inducing activity on Adriamycin-treated cancer cell, *J. Nat. Med.* (2021), <https://doi.org/10.1007/s11418-021-01528-8>.
- T. Matsumoto, T. Kitagawa, D. Imahori, H. Yoshikawa, M. Okayama, M. Kobayashi, N. Kojima, M. Yamashita, T. Watanabe, Cell death-inducing activities via Hsp inhibition of the sesquiterpenes isolated from *Valeriana fauriei*, *J. Nat. Med.* (2021), 0123456789, <https://doi.org/10.1007/s11418-021-01543-9>.
- C.Y. Peng, J.Q. Liu, R. Zhang, J.C. Shu, A new alkaloid from the fruit of *Nandina domestica* Thunb, *Nat. Prod. Res.* 28 (15) (2014) 1159–1164, <https://doi.org/10.1080/14786419.2014.921166>.
- T. Kodai, Y. Horiuchi, Y. Nishioka, N. Noda, Novel cycloartane-type triterpenoid from the fruits of *Nandina domestica*, *J. Nat. Med.* 64 (2) (2010) 216–218, <https://doi.org/10.1007/s11418-010-0389-6>.
- V.K. Bajpai, I.W. Park, J.I. Lee, S. Shukla, S.H. Nile, H.S. Chun, I. Khan, S.Y. Oh, H. Lee, Y.S. Huh, M.K. Na, Y.K. Han, Antioxidant and antimicrobial efficacy of a biflavonoid, amentoflavone from *Nandina domestica* in vitro and in minced chicken meat and apple juice food models, *Food Chem.* 271 (July 2018) (2019) 239–247, <https://doi.org/10.1016/j.foodchem.2018.07.159>.
- A. Yajima, Y. Oono, R. Nakagawa, T. Nukada, G. Yabuta, A simple synthesis of four stereoisomers of roseoside and their inhibitory activity on leukotriene release from mice bone marrow-derived cultured mast cells, *Bioorg. Med. Chem.* 17 (1) (2009) 189–194, <https://doi.org/10.1016/j.bmc.2008.11.002>.
- B. D'Ambrosia, M. DellaGreca, A. Fiorentino, P. Monaco, P. Oriano, F. Temussi, Structure elucidation and phytotoxicity of C13 nor-isoprenoids from *Cestrum parqui*, *Phytochemistry* 65 (4) (2004) 497–505, <https://doi.org/10.1016/j.phytochem.2003.11.018>.
- H. Kai, M. Baba, T. Okuyama, Two new megastigmanes from the leaves of *Cucumis sativus*, *Chem. Pharm. Bull.* 55 (1) (2007) 133–136, <https://doi.org/10.1248/cpb.55.133>.
- Y.H. Hong, S.C. Wang, C. Hsu, B.F. Lin, Y.H. Kuo, C.J. Huang, Phytoestrogenic compounds in alfalfa sprout (*Medicago sativa*) beyond coumestrol, *J. Agric. Food Chem.* 59 (1) (2011) 131–137, <https://doi.org/10.1021/jf102997p>.
- R.R. Kulkarni, W. Lee, T.S. Jang, J.I. Lee, S. Kwak, M.S. Park, H.S. Lee, J.S. Bae, M. K. Na, Caffeoyl glucosides from *Nandina domestica* inhibit LPS-induced endothelial inflammatory responses, *Bioorg. Med. Chem. Lett.* 25 (22) (2015) 5367–5371, <https://doi.org/10.1016/j.bmcl.2015.09.031>.
- His-Jung Yu, Chien-Chih Chen, Bor-Jinn Shieh, Two new constituents from the leaves of *Magnolia coco*, *J. Nat. Prod.* 61 (8) (1998) 1017–1019, <https://doi.org/10.1021/np970571d>.
- M. Hellwig, T. Henle, Baking, ageing, diabetes: a short history of the maillard reaction, *Angew. Chem. Int. Ed.* 53 (39) (2014) 10316–10329, <https://doi.org/10.1002/anie.201308808>.
- Y. Yamano, M. Ito, Synthesis of optically active vomifoliol and roseoside stereoisomers, *Chem. Pharm. Bull.* 53 (5) (2005) 541–546, <https://doi.org/10.1248/cpb.53.541>.
- T. Matsumoto, S. Nakamura, S. Nakashima, T. Ohta, K. Ogawa, M. Fukaya, J. Tsukioka, T. Hasei, T. Watanabe, H. Matsuda, Neolignan and megastigmane glucosides from the aerial parts of *Isodon japonicus* with cell protective effects on BaP-induced cytotoxicity, *Phytochemistry* 137 (2017) 101–108, <https://doi.org/10.1016/j.phytochem.2017.02.007>.
- Y. Kraepiel, P. Roussel, B. Sotta, L. Kerhoas, J. Einhorn, M. Caboche, E. Miginiac, Analysis of phytochrome-and ABA-deficient mutants suggests that ABA degradation is controlled by light in *Nicotiana plumbaginifolia*, *Plant J.* 6 (5) (1994) 665–672, <https://doi.org/10.1046/j.1365-313X.1994.6050665.x>.
- T. Matsumoto, D. Imahori, K. Achiwa, Y. Saito, T. Ohta, T. Yoshida, N. Kojima, M. Yamashita, Y. Nakayama, T. Watanabe, Chemical structures and cytotoxic activities of the constituents isolated from *Hibiscus tiliaceus*, *Fitoterapia* (2020) 142, <https://doi.org/10.1016/j.fitote.2020.104524>.
- J. Schneider, M.M. Centeno, F.J. Rodriguez-Escudero, T. Efferth, J. Mattern, M. Volm, High rate of expression of multidrug resistance-associated P-glycoprotein in human endometrial carcinoma and normal endometrial tissue, *Eur. J. Cancer* 29 (4) (1993) 554–558, [https://doi.org/10.1016/S0959-8049\(05\)80150-9](https://doi.org/10.1016/S0959-8049(05)80150-9).
- S.V. Ambudkar, C. Kimchi-Sarfaty, Z.E. Sauna, M.M. Gottesman, P-glycoprotein: from genomics to mechanism, *Oncogene* 22 (47) (2003) 7468–7485, <https://doi.org/10.1038/sj.onc.1206948>.
- C.E. Grant, G. Valdimarsson, D.R. Hipfner, K.C. Almquist, S.P.C. Cole, R.G. Deeley, Overexpression of multidrug resistance-associated protein (MRP) increases resistance to natural product drugs, *Cancer Res.* 54 (2) (1994) 357–361.
- J.D. Allen, R.F. Brinkhuis, L. Van Deemter, J. Wijnholds, A.H. Schinkel, Extensive contribution of the multidrug transporters P-glycoprotein and Mrp1 to basal drug resistance, *Cancer Res.* 60 (20) (2000) 5761–5766.
- S. Shukla, Z.S. Chen, S.V. Ambudkar, Tyrosine kinase inhibitors as modulators of ABC transporter-mediated drug resistance, *Drug Resist. Updat.* 15 (1–2) (2012) 70–80, <https://doi.org/10.1016/j.drug.2012.01.005>.
- L.J. Goldstein, H. Galski, A. Fojo, M. Willingham, S.L. Lai, A. Gazdar, R. Pirker, A. Green, W. Crist, G.M. Brodeur, M. Lieber, J. Cossman, M.M. Gottesman, I. Pastan, Expression of multidrug resistance gene in human cancers, *J. Natl. Cancer Inst.* 81 (2) (1989) 116–124, <https://doi.org/10.1093/jnci/81.2.116>.
- C.P. Wu, S. Lusvardi, S.H. Hsiao, T.C. Liu, Y.Q. Li, Y.H. Huang, T.H. Hung, S. V. Ambudkar, Licochalcone a selectively Resensitizes ABCG2-overexpressing multidrug-resistant Cancer cells to chemotherapeutic drugs, *J. Nat. Prod.* 83 (5) (2020) 1461–1472, <https://doi.org/10.1021/acs.jnatprod.9b01022>.
- V.C. Jacqueline, Gouaze-andresson Valerie, C.C. Myles, Expression of P-glycoprotein in HeLa cells confers resistance to ceramide cytotoxicity, *Int. J. Oncol.* 37 (6) (2010) 1591–1597, <https://doi.org/10.3892/ijo.00000813>.
- E. Santoni-Rugiu, J.A. Silverman, Functional characterization of the rat mdr1b encoded P-glycoprotein: not all inducing agents are substrates, *Carcinogenesis* 18 (11) (1997) 2255–2263, <https://doi.org/10.1093/carcin/18.11.2255>.
- T. Tsuruo, H. Lida, S. Tsukagoshi, Y. Sakurai, Overcoming of vincristine resistance in p388 leukemia in vivo and in vitro through enhanced cytotoxicity of vincristine and vinblastine by verapamil, *Cancer Res.* 41 (5) (1981) 1967–1972.
- Wavefunction Inc.: Irvine, CA.
- M.J. Frisch, G.W. Trucks, H.B. Schlegel, G.E. Scuseria, M.A. Robb, J.R. Cheeseman, G. Scalmani, V. Barone, G.A. Petersson, H. Nakatsuji, X. Li, M. Caricato, A. V. Marenich, J. Bloino, B.G. Janesko, R. Gomperts, B. Mennucci, H.P. Hratchian, J. V. Ortiz, A.F. Izmaylov, J.L. Sonnenberg, D. Williams-Young, F. Ding, F. Lipparini, F. Egidi, J. Goings, B. Peng, A. Petrone, T. Henderson, D. Ranasinghe, V. G. Zakrzewski, J. Gao, N. Rega, G. Zheng, W. Liang, M. Hada, M. Ehara, K. Toyota, R. Fukuda, J. Hasegawa, M. Ishida, T. Nakajima, Y. Honda, O. Kitao, H. Nakai, T. Vreven, K. Throssell, J.A. Montgomery Jr., J.E. Peralta, F. Ogliaro, M. J. Bearpark, J.J. Heyd, E.N. Brothers, K.N. Kudin, V.N. Staroverov, T.A. Keith, R. Kobayashi, J. Normand, K. Raghavachari, A.P. Rendell, J.C. Burant, S.S. Iyengar, J. Tomasi, M. Cossi, J.M. Millam, M. Klene, C. Adamo, R. Cammi, J.W. Ochterski, R.L. Martin, K. Morokuma, O. Farkas, J.B. Foresman, D.J. Fox, Gaussian 16, Revision A.03, Gaussian, Inc, Wallingford, CT, 2016.
- T. Bruhn, A. Schaumlöf, Y. Hemberger, G. Pecitelli, SpecDis: quantifying the comparison of calculated and experimental electronic circular dichroism spectra, *Chirality* 25 (4) (2013) 243–249, <https://doi.org/10.1002/chir.22138>.